IOP Conf. Series: Journal of Physics: Conf. Series **876** (2017) 012016 doi:10.1088/1742-6596/876/1/012016

Main Nuclear Physics requirements for the robustness of r-process nucleosynthesis calculations in slow ejecta from neutron-star mergers (NSM)

J J Mendoza-Temis[1,2] and A Frank[1,2]

[1]Instituto de Ciencias Nucleares, Universidad Nacional Autónoma de México, 04510 México, D.F., México
[2]Centro de Ciencias de la Complejidad, Universidad Nacional Autónoma de México, 04510 México, D.F., México

E-mail: joel.mendoza@correo.nucleares.unam.mx

Abstract. Here we deal with r-process nucleosynthesis simulations for matter ejected dynamically in NSM, recently a number of such simulations (see [1, 2, 3, 4]) have display a robust pattern in their final yields. It is the main goal of this contribution to address at the main requirements from the nuclear physics point of view in order to guarantee a robust pattern in the final r-process abundances for mass numbers $A > 120$. Our results suggest that one can achieve such behaviour for slow ejecta from neutron-star mergers as long as fission cycling is involved. On the other hand, using a representative r-process calculation as a working example, we explored the main stages in the evolution of an r-process. Finally, we conclude that fine tunning of local features in the pattern of final yields (2nd, rare earth and 3rd r-process peaks) depend on an interplay between the mass surface and other nuclear structure properties involved.

1. Introduction

There is no doubt that one of the most interesting open questions is that of how nature builds its elements. Nuclear structure properties, in particular nuclear masses, particle capture rates, β-decay and fission are the most important ingredients to elucidate this question. The so-called rapid neutron-capture process (r-process), is known to be at the origin of approximately half of the $A > 60$ stable nuclei observed in nature. It is commonly accepted that the r-process occurs as a sequence of neutron captures and β-decays in environments with extreme neutron densities, under such physical conditions matter reaches a region farther away from stability, which makes the calculation of the r-process harder that it seems, because so far only a few of the required nuclear structure properties are experimentally known, consecuently almost the entire set have to rely on theoretical grounds. And, on top of that, the astrophysical site of the r-process remains unindentified. For many years the neutrino-driven wind from the surface of a freshly born neutron star in a corecollapse supernova has been the favored site [5]. However, recent supernova simulations [6] indicate that the conditions of the matter ejected in the wind (entropy, expansion velocity, proton-to-neutron ratio) are not suited to support an r-process which produces the elements in the third peak (around mass number A$\sim$195) and beyond. We have performed r-process simulations based on recent numerical simulations of NSM, which indicate that the matter ejected during the dynamical phase is very neutron rich with extremely

large neutron-to-seed ratios ($R_{n/s} > 400$) [1, 2, 3]; i.e. there are many neutrons which can be captured by seed nuclei transporting matter to very heavy nuclei in the region of the nuclear chart where decay by fission is possible. Our work is organized as follows. In the next section we give a brief description the main nuclear physics input required to performed r-process calculations. Then in section 3, we introduce a working example to understand the relavant stages in evolution of an r-process from the nuclear physics point of view. The Results of our simulations are presented and discussed in section 4. Finally, we conclude in section 5.

2. Nuclear physics input

Nuclei are particularly complex systems, ranging from a single proton to more than three hundred nucleons; too large for a detailed microscopic treatment but too small for statistical methods. Interest in them is not restricted to nuclear physicists because the atomic nuclei that constitute our world are manufactured inside stars, defining their evolution and fate. In this contribution we are mainly interested in performing r-process calculations. The main nuclear physics properties required to achive our goal are: nuclear masses, reaction rates, such as n-capture (n, γ), phodissociation (γ, n), β-decay, and rates for neutron induced and β-delayed fission, as well as the corresponding fission fragment distributions. In what follows, a brief description of each of them will be provided.

2.1. Nuclear masses

Arguably, the most basic property of a nucleus is its mass. Understanding nuclear masses provides a test of our basic knowledge of nuclear structure and is an essential ingredient of the fundamental astrophysical problem of nucleosynthesis, which often takes place in far-from-stability conditions, on ultrashort time scales [7]. Though great progress has been made on measurement the mass of short-lived nuclei that are far from the region of stable, naturally occurring isotopes, theory is needed to predict their properties and guide experiments that search, for example, for regions of increased stability [8]. Even when most of the r-process nuclei are not yet reachable by up-today facilities, experimental mesurements are still needed, on the one hand for validating theoretical mass models, and on the other as inputs for r-process models. The efforts to calculate nuclear masses have been hampered by the absence of a true effective theory of the nuclear interaction and by the difficulties inherent to quantum manybody calculations. Instead, simplified approaches to model the atomic nucleus have been devised. The predictions made by different models often turn out to agree in regions where masses are available, but diverge profoundly away from known regions. Reliable theoretical models and methodologies that can predict the mass and other properties of these exotic nuclei are still missing [9]. In summary, Nuclear masses are particularly important as they, via the neutron separation energies, define the r-process path in the nuclear chart and secondly they are crucial ingredients in the statistical model calculation of neutron capture cross sections. The impact of a number of theoretical nuclear mass models (FRDM [10], HFB21 [11], WS3 [12], DZ31 [13, 14] and range of possible Skyrme functionals within the DFT framework) for the calculation of the neutron capture rates that enter in the r-process simulations has been widely explored in previous works (see [4, 15] for more details). Another approach is through Monte Carlo simulations, in which nuclear masses are randomly varied within experimental or estimated theoretical uncertainties, such studies suggest that in order for details of the abundance patterns to stand out over nuclear uncertainties, a mass precision of 100 keV. [16]. Unfornately, the overall RMS deviation between theoretical and experimental masses for the range A=16-270 is 500 keV or greater. As the descripton of the so called "deformed nuclei" is one of the main sources of discrepancies among all theoretical mass models, and as their predictions are relevant for r-process calculations, in what follows we will briefly discuss this issue.

2.1.1. The region of transition from spherical to deformed nuclei. Regardless of the theoretical approach used for the calculation of the nuclear masses and important feature that all the models shared is the deformation. To display the predicted "deformed nuclei region" for a number of selected mass models, we are going to use the two neutron separation energies ($S_{2n}/2$), because it is well known, that they mostly display an smooth behaviour except in regions where shell closures or the onset of deformation is present. In Fig. 1, we display $S_{2n}/2$ as a function of the mass number A for isotopic chains ranging from $30 < Z < 92$. The experimental values of $S_{2n}/2$ are always included when available, and displayed by red lines. In the absence of experimental information, the theoretical values are displayed by black lines. The predicted deformed regions are added and identified by green lines on top of the theoretical value of $S_{2n}/2$. Finally every 5 isotopic chains bluish lines are included only to guide the eye. To stress the need of theoretical predictions and as a reminder, let us consider the waiting point approximation [17], assuming typical r-process conditions, i.e., $T_9 = 1$ GK and $n_n = 10^{24}\ cm^{-3}$, we obtain an r-process path of $S_n^0 = S_{2n}/2 \approx 2$ MeV, meaning that most of relevant nuclei for r-process calculations lie not only in the extrapolated region but also in the "deformed region" (see purple box region in Fig. 1). Concerning to the predicted $S_{2n}/2$ surfaces (see black and green lines in Fig. 1), the first thing to glimpse the eye is the extremely irregular behavior of the predicted surfaces by HFB21 and FRDM in comparison to those of WS3 and DZ31. In addition, in between the shell closures (which in this representation appear as vertical lines) there are two regions, namely for $90 < A < 110$ and for $130 < A < 170$, where most of the selected models predict an onset of deformation (see green lines in Fig. 1). From the nuclear physics point of view, this piece of information is of vital relevance to understand the evolution of an r-process.

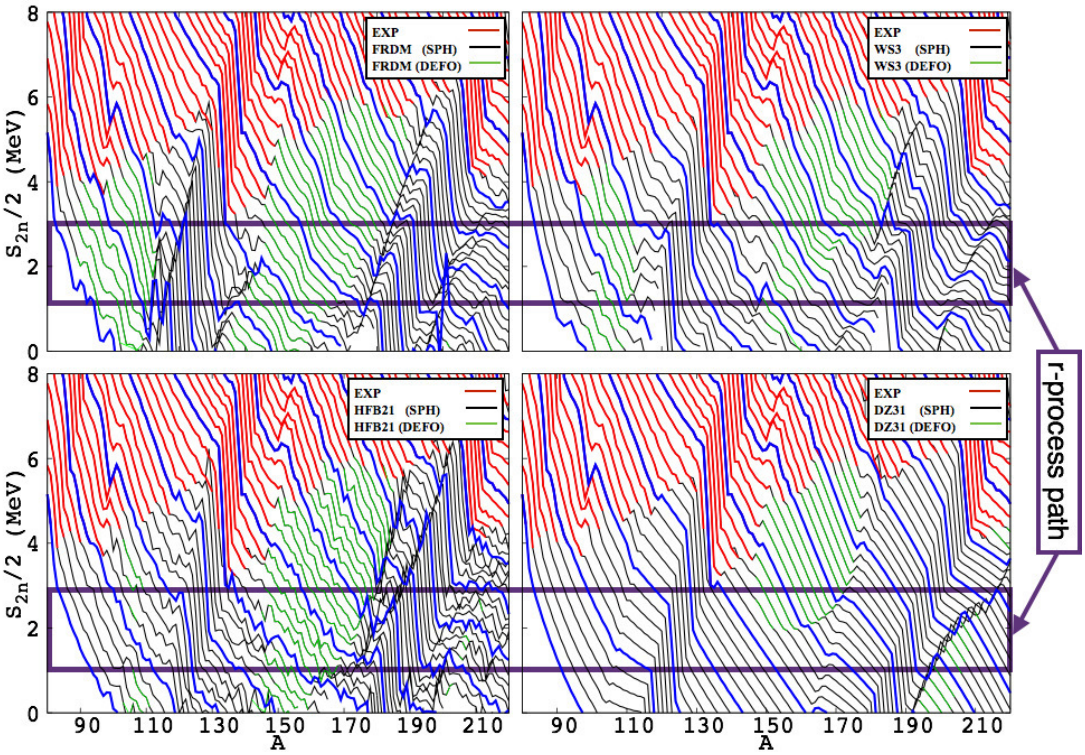

Figure 1: (Color online) $S_{2n}/2$ for a number of isotopic chains ($30 < Z < 92$) based on a number of mass models (see black lines). Experimental data is always shown with red lines. Well deformed nuclei are displayed with green lines. Blue lines are added every five isotopic chains to guide the eye. Relevant nuclei on the r-process path are denoted by a purple box.

2.2. Reaction rates

A key ingredient in any astrophysical calculations is the knowledge of the thermonuclear reaction rates via their cross sections; as they measure the probability of reactions between a target nucleus and incoming projectiles under astrophysical conditions. The commonly used tool to generate theoretical reaction rates for r-process rely on the Hauser-Feshbach theory [18], where all energetically possible reaction channels are in statistical competition with a probability evaluated by dividing over the sum of transmission coefficients for all channels as in Eq. 1, where T is the transmission coefficient, J^π the spin and parity of each populated level, and E is the energy at which the reaction is evaluated. The subscript c denotes the formation of a compound nucleus while the index i runs over all possible exit channels for the decay of the compound system.

$$\sigma(E) = \Sigma_{J^\pi} \frac{T_c(J^\pi) T_\gamma(J^\pi)}{\Sigma_i T_i(J^\pi)} \tag{1}$$

This picture, is suitable for the description of reactions involving the decay of nuclei excited at a sufficiently high energy to contain a large number of levels per MeV. When this condition is true an energy-averaged reaction cross section in this region of highly overlapping resonances is meaningful. Assuming that this condition is met, the main sources of physics-related uncertainty in the calculated reaction rates come from the modeling of the formation and decay of the excited compound nucleus through the respective transmission coefficients. These are calculated using nuclear level densities to describe the excitation of each compound nucleus, optical potentials to describe the emission or absorption of particles, and γ-ray strength functions to describe the emission of γ-rays [19].

2.3. β-decays

Besides masses and reaction rates, the β-decay half-lives are an important physical ingredient to perform r-process nucleosynthesis simulations. They must be known all over the nuclear chart, but particularly in the region between the valley of stability and the r-process equilibrium path. While masses determine the route of r-process under given astrophysical conditions, the β-decay half-lives of waiting-point nuclei dictate how fast the process can proceed towards heavy nuclei and how much material is accumulated in a given isotopic chain. In other words, the effective r-process timescale can be affected by modifications of individual β-decay half-lives that so far are based on relatively uncertain theoretical approaches [20, 21]. As an example, of the relevance of β-decays half-lives, the competition between β-decay and n-capture (n, γ) in the region A$\sim$160 during freeze-out stage can have significant consequences for the formation of a small but pronounced rare-earth peak [22, 23]. In addition, during freeze-out and because of neutron capture rates are not fast anymore, β-delayed neutron emission takes place changing the isobaric decay chain towards stability.

2.4. Fission

Fission rates and fragment distribution of neutron-rich heavy nuclei are required to understand r-process nucleosynthesis, specially at late-time r-process dynamics through the so-called recycling mechanism [24, 25]. Under NSM conditions fission cycling is unavoidable due to the large neutron-to-seed ratios ($R_{n/s}$) reached in their ejecta, in addition fission is also an important source of free neutrons, under r-process conditions the total number of neutrons produced can be divided into two components: 1) a prompt component that consists of the neutrons evaporated mainly by the highly excited fragments, and 2) a delayed component that occurs during the decay of the fragments to the instantaneous r-process path. Unfortunately, a comprehensive, microscopic explanation of nuclear fission still eludes us due to the complexity of the process. This fundamental nuclear decay is an example of a quantal large-amplitude collective motion [26].

3. Numerical Simulations. Description of a working example.

Previously in [4], we have performed a number of simulations to explore the impact of nuclear masses in r-process nucleosynthesis, covering the full range of ejecta coming from a 3D simulation of NSM [27]. As the current work is intended to understand the nuclear physics occurring at relevant stages of the evolution of an r-process, we decided to use a working example, in which a representative trajectory for slow ejecta from NSM has been taken, such trajectory characterizes by being highly neutron-rich ($Y_e \sim 0.05$), and having a neutron-to-seed ration $R_{n/s} \sim 650$, favouring an initial composition from Nuclear Statistical Equilibium (NSE) centering at $A \sim 120$. Concerning the Nuclear physics input, our calculations consider a nuclear network already available [4], where as nuclear reactions we considered charge particle reactions, neutron captures and its inverse process, photo-dissociation, and β and α-decay and fission. In [4, 28], we have derived the neutron capture rates consistently for a number of mass model within the statistical model using the code MOD-Smoker (see [30] which includes changes and updates from the code NONSMOKER due to Rauscher and Thielemann [31]), along this working example, we decided to choose the theoretical binding energies from DZ31, because the physics behind this model is the more familiar to the authors (see [14]), and most important, we prefer to deal with DZ31 mass predictions that display a smoother mass surface far from stability (see Fig. 1) than with a noisy mass surface (as predicted by most models) which could be attributed to numerical noise rather than physics. The photodissociation rates were obtained from the neutron capture rates by detailed balance. For nuclei, for which the half lives are not known experimentally, we have adopted the β-decay (and β-delayed neutron emission) rates from the compilation of Möller *et al.* [20], which was derived from QRPA calculations on top of the FRDM mass model. We used the parametrization of Ref. [32] of the Viola-Seaborg formula to estimate the α-decay rates, which become relevant for heavy nuclei beyond lead. Finally, for nuclei with $Z > 83$, where a competition between (n, γ) and neutron induced fission can take place, we used neutron-induced reaction rates taken from [33] that are based on the FRDM mass model [10] and the Thomas-Fermi fission barriers of Myers and Swiatecki [34]. Rates for β-delayed and spontaneous fission were adopted from [35]. Our fission yields were taken from the calculations of Ref. [36] which were derived using the code ABLA. This approach also gives a consistent estimate for the number of neutrons set free during the fission process.

4. Results at relevant stages of an r-process

Figs. 2 to 4, shown r-process nucleosynthesis results for our prevously described working example at 3 different phases of the evolution :

(a) at freeze-out, which we define as the moment where $R_{n/s} = 1$,
(b) at the moment when β-decays becomes the dominant process ($\tau_{(n,\gamma)} >> \tau_\beta$) as there are not enough neutrons ($R_{n/s} \sim 10^{-10}$), and
(c) at the final abundance, calculated at a time of 1 Gyr.

To better interpet our findings, we have decided to plot r-process abundaces (red lines for DZ31, and blue dots for solar) as a function of atomic number A (see upper panel on l.h.s. in Figs. 2 to 4), and a color coded version of the same on the N-Z plane (see r.h.s. in Figs. 2 to 4, where stable isotopes are addead as black empty boxes). To understand the relevant nuclear physics, we added the instantaneous r-process path, on top of the $S_{2n}/2$ (previouly described in Fig. 1), where black dots represent the most abundant isotope for a given isotopic chain Z (see lower panel on l.h.s. in Figs. 2 to 4). In addition to discuss the relevant regions of the landscape, where the evolution of an r-process is taking place we added circles with numbers inside.

4.1. freeze-out

As initially matter is highly neutron rich, the dominant process is that of n-capture. When the r-process reaches the freeze-out, the abundances show a strong odd-even staggering (see upper panel in Fig. 2), matter is mostly halted at neutron shell closures (see lower panel in Fig. 2), namely at N=126 (A∼190) and N=184 (A∼280), which translates in troughs in the abundance pattern right after those major shell closures. The amount of material accumulated in the fissioning region, A>240 is much larger than the one present in the region below the 3rd r-process peak, this occurs because the flux of matter is determine by β-decay half-lives, and as τ_β(N=184)>τ_β(N=126) matter stays longer in the transuranium region (A>240). There are 3 regions of interest:

1. **Region between 2nd and 3rd r-process peak (130<A<180).** As it is shown by the r-process path (black dots in lower panel in Fig. 2), the odd-even staggering in abundances are due to local effects induced by a sudden change in the intrinsic deformation starting at N=90 (A∼140) (green lines in lower panel in Fig. 2) and the onset of a sub-shell at N=112 (A∼160) which produces another trough in the abundances. The latter effects depends on the mass model.
2. **Region after 3rd r-process peak (200<A<240).** Local features in the abundances are explained in the same way as in item 1. In this region, deformation sets in at N=130 (A∼200), and the sub-shell is located at N∼150 (A∼230).
3. **Transuranium region (A>240).** There is a sub-shell at N∼170 (A∼260) which produces a notorius trough in abundances. Nuclei located at N=184 (A∼280) have lower barriers and consecuently n-induced fission dominates over n-capture, and the r-process cycles to medium mass nuclei rather than producing heavier nuclei.

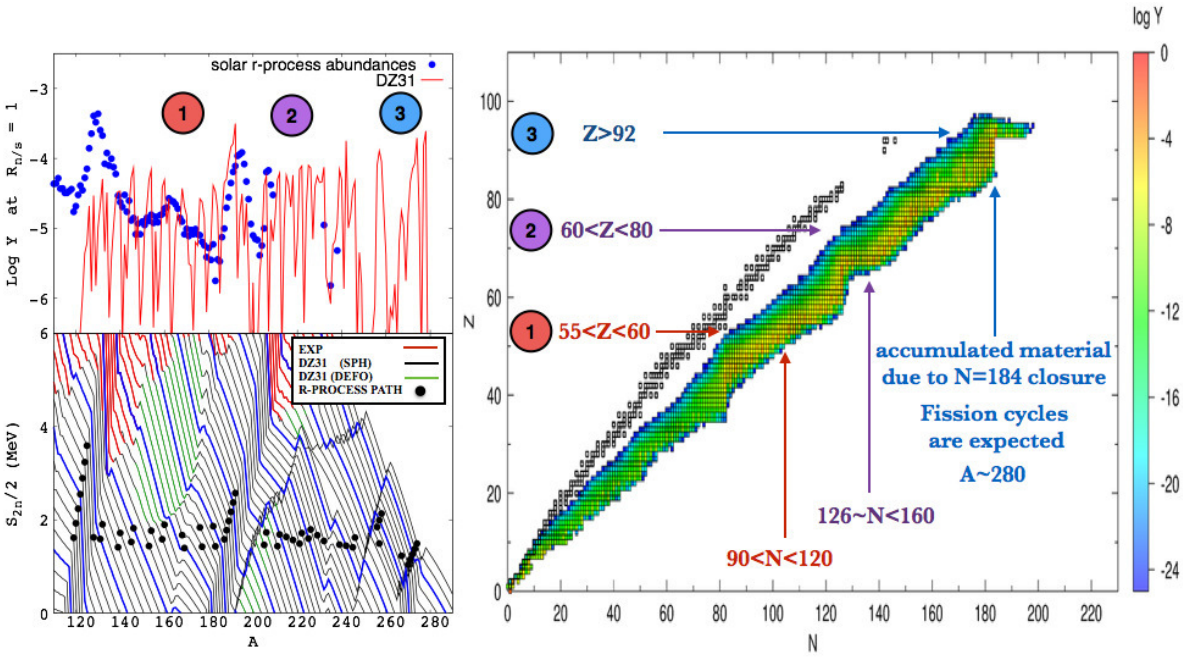

Figure 2: (Color online) Red lines display r-process abundances as a function of mass number at freeze-out stage, for a representative slow ejecta from NSM and masses taken from DZ31, solar abundances as blue dots for comparison (see upper panel l.h.s.). $S_{2n}/2$ surfaces, as described in fig. 1, and on top of them black dots representing the r-process path (see lower panel l.h.s.). Color coded Abundances on N-Z landscape and stable isotopes as black empty boxes (see r.h.s.).

4.2. beta-decay phase

Once neutron captures are slower than β-decays, matter decays to stability. In particular, at this stage, the remarkable features of the r-process abundance pattern, namely the 2nd peak, the rare earth peak, and the 3rd peak appear almost at the right height and place (see upper panel on l.h.s in Fig. 3). There are 5 regions to be consider:

1. **2nd r-process peak (A$\sim$130).** The fission fragment ditribution for nuclei at A$\sim$280 predicted by ABLA code [36] (see r.h.s in Fig. 3) shows that the origin of this peak is mainly due to fission cycling, as one of its fragments, precisely lie at A$\sim$130. The position of the peak is slighly shifted to the right due to late-time n-captures.
2. **Region around (A$\sim$140).** This kink in the abundances is produced both, by matter halted at N=82 and by fission, as the 2nd fission fragment for nuclei at A$\sim$280 predicted by ABLA code [36] mostly lie at A$\sim$140.
3. **rare earth peak (A$\sim$160).** This peak is mainly produced by the competition between β-decay and n-capture (n,γ) in the region A$\sim$160 soon after the freeze-out [22, 23]. Our results suggest, that at this stage, the instantaneous r-process path at A$\sim$160 lies in the region of transition from spherical to deformed nuclei (green lines in lower panel on l.h.s. in Fig. 3), which makes this peak very sensitive to the mass model being used.
4. **3rd r-process peak (A$\sim$195).** The origin of this peak is matter halted at N=126 expose to late-time n-captures. It turned-out that this peak is wider than expected, because there is a sub-shell effect at N=112 (A$\sim$180) which is mainly accumulating material. Again, our findings suggest that this peak is very sensitive to the mass model being used.
5. **Region above Lead A>208.** The significant amount of matter above lead still existing (see upper panel on l.h.s. in Fig. 3 and on r.h.s. in Fig. 4), will mostly decays via α-decay to finally form the lead peak. To estimate the α-decay rates, we have made used of [32].

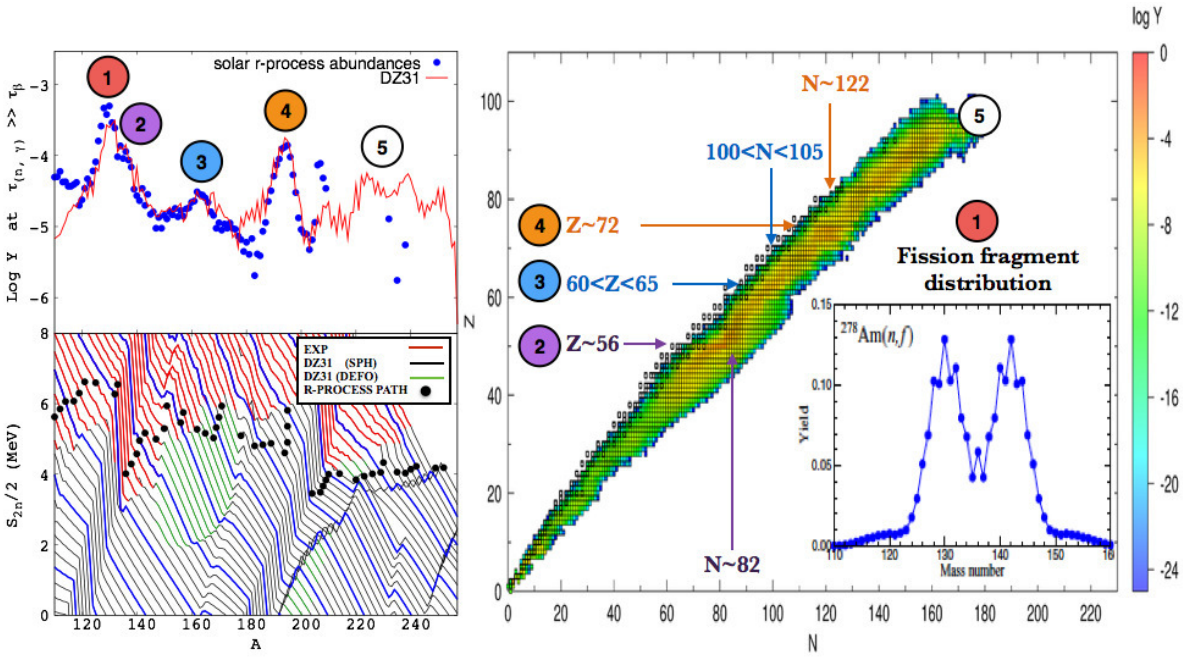

Figure 3: (Color online) r-process abundances when β-decay becomes the dominant process, same description as Fig. 2. Fission fragment distributions as function of mass number for neutron induced fission on ^{278}Am as predicted by the ABLA code are added on r.h.s.

4.3. final abundances at 1GY

We noticed that the final abundances at 1 Gyr are smoother due to late-time n-captures coming from fission and subsequent β-decay and photodissociation. When comparing with solar abundances, we noticed that overall the main features of r-process abundances pattern at 1 GY are well reproduced (see upper panel on l.h.s in Fig 4). The slighly differences at the 2nd, at the rare earth peak and at the 3rd r-process peak has been explained in subsection 4.2. The color coded version of the abundances on the N-Z plane shows nuclei responsible for the above mentioned r-process peaks (see r.h.s. in Fig. 4). Finally, there is an over-estimation in both the Lead Peak (A$\sim$208) and in the abundances associated with the long-lived Thorium and Uranium isotopes (A>230).

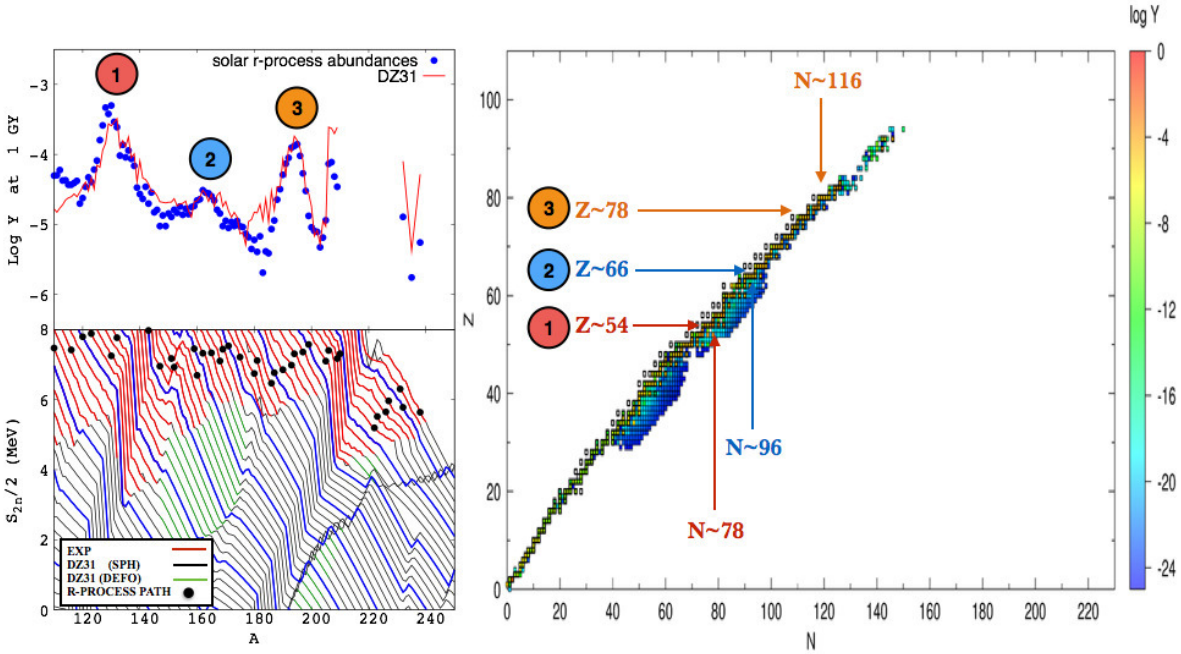

Figure 4: (Color online) r-process abundances at 1 GY, same description as Fig. 2

4.4. On the robustness of r-process abundances

Up to now, we have only dealt with our working example to gain insight on relevant nuclear physics at different stages of the evolution of an r-process, however a remarkable result we have found in [4] is worth to be mentioned: "...When considered only the so-called "slow ejecta", the most striking feature of our calculations is the fact that the final abundances for mass numbers A>120 are virtually identical, for a given mass model." (see Fig. 5). In what follows a few words on the impact of nuclear masses in the final r-process abundances would be stated.

As we have noticed the 2nd r-process peak is due to fission fragments coming from A$\sim$280 hence its origin is independet of the mass model being used; soon afterwards neutron captures on the fission yields are responsible for a flow of matter from the 2nd r-process peak to heavier nuclei. This mechanism operates in all used mass models except in FRDM due to the fact that material is halted at N$\sim$90, this feature translates in a notorious over-estimation of the 2nd r-process peak, which is also shifted to the right (see upper leftmost panel in Fig 5).

To understad the behavior around the 3rd r-process peak, table 1 shows the one-neutron separation energies (S_{1n}) predicted by a number of mass models for the nuclei ^{199}Yb, ^{198}Tm and ^{197}Er (all with N=129, just above the magic number N=126). The FRDM and HFB21 mass

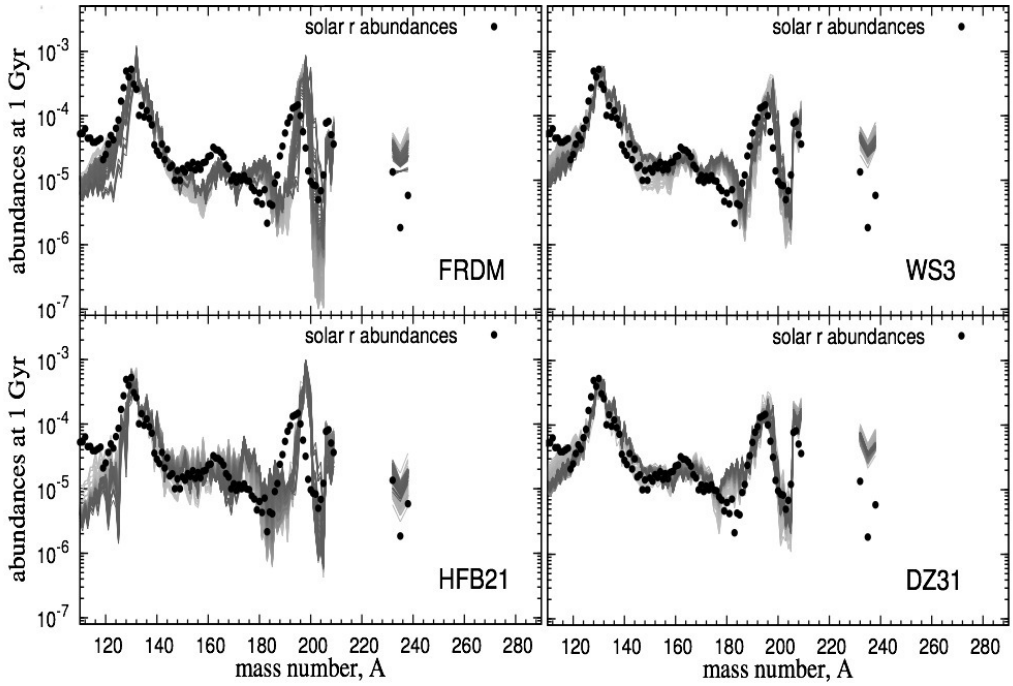

Figure 5: (Color online) Final r-process abundances at a time of 1 Gyr for the different mass models and all the slow ejecta trajectories.

models predict noticeably smaller neutron separation energies than the DZ31 or the WS3 models in this mass range. Thus these nuclei act as (additional) obstacles in r-process simulations using the FRDM and HFB21 mass models, even if the mass flow has overcome the $N = 126$ waiting points. As a result, the third peak in the abundance distribution is shifted for these two mass models to higher mass numbers as can be seen in Fig. 5 caused mainly by late-time neutron captures. Due to the larger neutron separation energies, the $N = 129$ nuclei do not act as obstacles in simulations adopting the Duflo-Zuker or WS3 mass models. Relatedly the third peak develops at $A \sim 195$, associated with the $N = 126$ waiting points.

Table 1: S_{1n} (in MeV) for a number of selected mass models, for the region N=129.

	^{199}Yb	^{198}Tm	^{197}Er
FRDM	0.52	0.62	0.26
HFB21	0.85	0.73	0.56
WS3	1.46	1.53	0.86
DZ31	1.39	1.48	0.81

5. Conclusions

We conclude that dynamical ejecta of NS mergers show a robust r-process pattern, as already concluded in refs. [1, 2, 3, 4], provided that the ejecta remains neutron rich, see refs [38, 39, 40]. The main requirement to achieve a robust r-process pattern is that the amount of material accumulated at freeze-out in the fissioning region, A$\gtrsim$240 is much larger than the one present in the region below the 3rd r-process peak. For the slow ejecta, this is guaranteed by the fact that the beta-decay half-lives grow with increasing mass number and by the presence of a neutron shell closure around $N = 184$. Both effects are responsible of producing a peak in the freeze-out

r-process abundances around A$\sim$280 (see upper panel on l.h.s. in Fig. 2). The material in this peak decays by fission contributing to the abundances around the 2nd r-process peak and producing a final robust r-process pattern. The rare earth peak and the 3rd peak abundances are noticeably more sensitive to nuclear masses that influence both the n-capture rates and the β-decay rates. It is not surprising that abundances of these peaks show a larger variation.

Acknowledgments

J.J. Mendoza-Temis is a DGAPA-UNAM fellow and thanks to DGAPA-PAPIIT project number IV100116 for its support.

References

[1] S Goriely, A Bauswein, and H-T Janka, Astrophys. J. **738**, L32 (2011).
[2] O Korobkin, S Rosswog, A Arcones, and C Winteler, Mon. Not. R. Astron. Soc. **426**, 1940 (2012).
[3] A Bauswein, S Goriely, and H-T Janka, Astrophys. J. **773**, 78 (2013).
[4] J J Mendoza-Temis, M R Wu, K Langanke, G Martínez-Pinedo, A Bauswein, and H-T Janka, Phys. Rev. C **92**, 055805 (2015).
[5] S. E. Woosley, J. R. Wilson, G. J. Mathews, R. D. Hoffman, and B. S. Meyer, Astrophys. J. **433**, 229 (1994).
[6] H.-T. Janka, Ann. Rev. of Nucl. Part. Sci. **62**, 407 (2012).
[7] C. E. Rolfs and W. S. Rodney, *Cauldrons in the Cosmos* (University of Chicago Press, Chicago, 1988).
[8] Y. Oganessian, Nature (London) **413**, 122 (2001).
[9] D. Lunney, J. M. Pearson, and C. Thibault, Rev. Mod. Phys. **75**, 1021 (2003).
[10] P Möller, J R Nix, W D Myers, and W J Swiatecki, At. Data Nucl. Data Tables **59**, 185 (1995).
[11] S Goriely, N Chamel, and J M Pearson, Phys. Rev. C **82**, 035804 (2010).
[12] M Liu, N Wang, Y Deng, and X Wu, Phys. Rev. C **84**, 014333 (2011).
[13] J Duflo and A P Zuker, Phys. Rev. C **52**, R23 (1995).
[14] J Mendoza-Temis, J G Hirsch, A P Zuker, Nuclear Physics A **843** (1), 14-36 (2010)
[15] D. Martin, A. Arcones, W. Nazarewicz, and E. Olsen, Phys. Rev. Lett. **116**, 121101 (2016).
[16] M. Mumpower, R. Surman, G.C. McLaughlin, and A. Aprahamian, Prog. Part. Nucl. Phys **86**, 86 (2016).
[17] A G W Cameron, J J Cowan, J W Truran, *Astrophysics and Space Science*, **91** 2 (1983).
[18] W. Hauser, and H. Feshbach, Phys. Rev., **87** 2 (1952).
[19] J. Pereira, *Private communication* (2016).
[20] P Mller, B Pfeiffer, and K-L Kratz, Phys. Rev. C **67**, 055802 (2003).
[21] T. Marketin, L. Huther, and G. Martnez-Pinedo, Phys. Rev. C **93**, 025805 (2016)
[22] R. Surman, J. Engel, J. R. Bennett, and B. S. Meyer, Phys. Rev. Lett. **79**, 1809 (1997)
[23] M. R. Mumpower, G. C. McLaughlin, and R. Surman, Phys. Rev. C **85**, 045801 (2012)
[24] G. Bell, Phys. Rev. **158** (1957)
[25] S. Goriely, J.-L. Sida, J.-F. Lemaître, S. Panebianco, N. Dubray, S. Hilaire, A. Bauswein, and H.-T. Janka, Phys. Rev. Lett. **111** 24 (2013)
[26] W. Nazarewicz, *Private communication* (2016).
[27] A Bauswein, H-T Janka, and R. Oechslin, Phys. Rev. D **82**, 08404 (2010).
[28] J. Mendoza-Temis, Ph.D. thesis, TU Darmstadt, (2014).
[29] J. M. Lattimer, Annu. Rev. Nucl. Part. Sci. **62**, 485 (2012).
[30] H. P. Loens, Diploma thesis. TU Darmstadt, (2007).
[31] T. Rauscher and F.-K. Thielemann F.-K., At. Data Nucl. Data Tables **75**, (2000).
[32] T Dong and Z Ren, Eur. Phys. J. A **26**, 69 (2005).
[33] I V Panov, I Y Korneev, T Rauscher, G Martínez-Pinedo, A Kelić-Heil, N T Zinner, and F-K Thielemann, Astron. Astrophys. **513**, A61 (2010).
[34] W D Myers and W J Swiatecki, Phys. Rev. C **60**, 014606 (1999).
[35] I Petermann, K Langanke, G Martínez-Pinedo, I V Panov, P-G Reinhard, and F-K Thielemann, Eur. Phys. J. A **48**, 122 (2012).
[36] N T Zinner, Ph.D. thesis, University of Aarhus, 2007 (unpublised).
[37] A Arcones and G Martínez-Pinedo, Phys. Rev. C **83**, 045809 (2011).
[38] S Wanajo, Y Sekiguchi, N Nishimura, K Kiuchi, K Kyutoku, and M Shibata, Astrophys. J. **789**, L39 (2014).
[39] Y Sekiguchi, K Kiuchi, K Kyutoku, and M Shibata, Phys. Rev. D **91**, 064059 (2015).
[40] S Goriely, A Bauswein, O Just, E Pllumbi, and H-T Janka, Mon. Not. R. Astron. Soc. **452**, 3894 (2015).
[41] S Goriely and G Martínez-Pinedo, Nucl. Phys. A **944** (2015).